Gastroenterology 2021;161:1924–1939

The Tight Junction Protein ZO-1 Is Dispensable for Barrier Function but Critical for Effective Mucosal Repair

Wei-Ting Kuo,[1,*] **Li Zuo**,[1,2,*] Matthew A. Odenwald,[3] Shariq Madha,[4] Gurminder Singh,[1] Christine B. Gurniak,[5] Clara Abraham,[6] and Jerrold R. Turner[1,3]

[1]Laboratory of Mucosal Barrier Pathobiology, Department of Pathology, Brigham and Women's Hospital and Harvard Medical School, Boston, Massachusetts; [2]Anhui Medical University, Hefei, Anhui, China; [3]Department of Pathology, The University of Chicago, Chicago, Illinois; [4]Department of Medical Oncology and Center for Functional Cancer Epigenetics, Dana-Farber Cancer Institute, Boston, Massachusetts; [5]Institute of Genetics, University of Bonn, Bonn, Germany; and [6]Department of Internal Medicine, Yale University, New Haven, Connecticut

This article has an accompanying continuing medical education activity, also eligible for MOC credit, on page e18. Learning Objective: Upon completion of this CME activity, successful learners will recognize that, despite being the first tight junction protein discovered, ZO-1 is not required for tight junction barrier function. They will also be able to explain how changes in intestinal epithelial ZO-1 expression is associated with colitis, identify the two noncanonical mechanisms by which ZO-1 promotes mucosal repair, and explain the hypothesis that ZO-1 loss contributes to defective mucosal healing in inflammatory bowel disease.

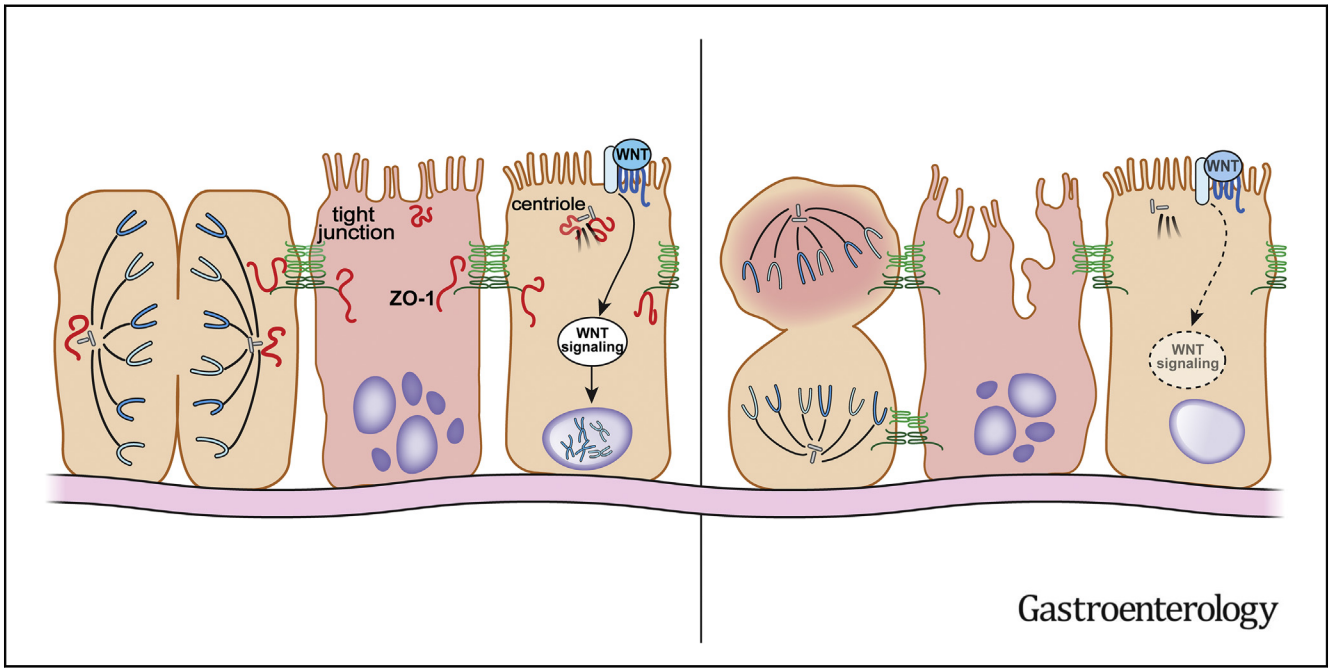

See editorial on page 1797.

BACKGROUNDS & AIMS: Increased permeability is implicated in the pathogenesis of intestinal disease. In vitro and in vivo studies have linked down-regulation of the scaffolding protein ZO-1, encoded by the *TJP1* gene, to increased tight junction permeability. This has not, however, been tested in vivo. Here, we assessed the contributions of ZO-1 to in vivo epithelial barrier function and mucosal homeostasis. **METHODS:** Public Gene Expression Omnibus data sets and biopsy specimens from patients with inflammatory bowel disease (IBD) and healthy control individuals were analyzed. $Tjp1^{f/f}$;vil-Cre^{Tg} mice with intestinal epithelial–specific ZO-1 knockout (ZO-$1^{KO.IEC}$) mice and $Tjp1^{f/f}$ mice littermates without Cre expression were studied using chemical and immune-mediated models of disease as well as colonic stem cell cultures. **RESULTS:** ZO-1 transcript and protein expression were reduced in biopsy specimens from patients with IBD. Despite mildly increased intestinal permeability, ZO-$1^{KO.IEC}$ mice were healthy and did not develop spontaneous disease. ZO-$1^{KO.IEC}$ mice were, however, hypersensitive to mucosal insults and displayed defective repair. Furthermore, ZO-1–deficient colonic epithelia failed to up-regulate proliferation in response to damage in vivo or Wnt signaling in vitro. ZO-1 was associated with centrioles in interphase cells and mitotic spindle poles during division. In the absence of ZO-1, mitotic spindles failed to correctly orient, resulting in mitotic catastrophe and abortive proliferation. ZO-1 is, therefore, critical for up-regulation of epithelial proliferation and successful completion of mitosis. **CONCLUSIONS:** ZO-1 makes critical, tight junction–independent contributions to Wnt signaling and mitotic spindle orientation. As a result, ZO-1 is essential for mucosal repair. We speculate that ZO-1 down-regulation may be one cause of ineffective mucosal healing in patients with IBD.

Keywords: Inflammatory Bowel Disease; Mitosis; Mitotic Spindle; Wnt; Intestinal Permeability.

Compromised intestinal barrier function, that is, increased intestinal permeability, has been hypothesized to be a Crohn's disease risk factor for more than 40 years. This was based on the observation that, among patients with Crohn's disease in remission, increased permeability is associated with relapse[1] as well as the identification of a subset of healthy first-degree relatives of Crohn's disease patients with increased intestinal permeability.[2] A recent study assessed intestinal permeability in such healthy first-degree relatives and found that their risk of developing Crohn's disease or ulcerative colitis was 50% greater than that of relatives with normal barrier function.[3] Thus, intestinal barrier dysfunction is a biomarker of IBD risk. Despite the central role of the tight junction in barrier regulation, the potential contributions of specific tight junction proteins to disease development, progression, and remission have, to date, only been inferred by correlating expression changes in small groups of patients with in vitro studies of cultured monolayers.[4–7]

To screen tight junction protein expression in an unbiased manner, we interrogated public data sets from patients with IBD and control individuals. We found consistent down-regulation of the tight junction scaffolding protein zonula occludens-1 (ZO-1) and confirmed this immunohistochemically. Further study using genetically modified mice identified previously unrecognized, yet critical, tight junction–independent ZO-1 contributions to Wnt–β-catenin signaling, mitotic spindle orientation, and effective epithelial repair.

WHAT YOU NEED TO KNOW

BACKGROUND AND CONTEXT

Intestinal barrier loss in patients with inflammatory bowel disease (IBD) is associated with reduced expression of the tight junction scaffold protein ZO-1, but the direct contributions of ZO-1 to barrier maintenance have not been studied in vivo.

NEW FINDINGS

ZO-1 expression was reduced in biopsy samples from patients with IBD. In mice, intestinal epithelial ZO-1 deletion modestly increases tight junction leak pathway permeability but does not cause profound barrier defects or spontaneous disease. Mucosal repair is, however, severely compromised in mice lacking intestinal epithelial ZO-1. This reflects defective Wnt–β-catenin signaling and aberrant mitotic spindle orientation, both of which may be related to the new observation that ZO-1 accumulate around centrioles.

LIMITATIONS

These studies were performed using human tissue samples and genetically modified mice. Further work is needed to define the mechanisms by which ZO-1 associates with centrioles, regulates mitotic spindle orientation, and promotes Wnt–β-catenin signaling. The impact of ZO-1 down-regulation on mucosal healing in human disease also requires further study.

IMPACT

ZO-1 down-regulation attenuates Wnt–β-catenin signaling and induces abortive epithelial proliferation to disrupt mucosal repair. Restoration of ZO-1 expression may promote healing.

Materials and Methods

Mouse studies followed protocols approved by institutional animal care and use committees and used vil-mRFP1-ZO-1 (Tg(Vil1-mRFP1/TJP1)#Tjr, MGI:5584023), *Tjp1*$^{f/f}$ (*Tjp1*$^{tm2c(KOMP)Wtsi}$, MGI:6272009), vil-Cre (B6.Cg-Tg(Vil1-cre)20Syr, MGI:3053819), vil-CreERT2 (B6.Cg-Tg(Vil1-cre/ERT2)23Syr/J, MGI:6278020), H2B-mCherry (R26-H2B-mCherry, CDB:CDB0239K), and GFP-β-actin (*Pfn1*$^{tm2.1(GFP/ACTB)Wit}$, MGI:5568700) mice. *Tjp1*$^{f/f}$ littermates were used as wild-type (WT) controls for *Tjp1*$^{f/f}$-vil-Cre (ZO-1$^{KO.IEC}$) mice. All experiments using mice were performed at least 3 times with similar results. Further experimental details are available in the Supplementary Methods.

Resource Sharing

Data, analytic methods, and study materials will be made available to academic investigators upon reasonable request.

Results

ZO-1 Expression Is Down-regulated in Inflammatory Bowel Disease

To comprehensively assess tight junction protein transcription in IBD, we screened the GDS3268 RNA microarray data set, which includes biopsy specimens from 67 patients with ulcerative colitis and 31 healthy control individuals.[8] This confirmed published results showing increased *CLDN1* and *CLDN2* and reduced *OCLN*, *CLDN4*, and *CLDN8* expression in ulcerative colitis (Figure 1*A*).[6,7] These changes were generally consistent across 5 additional ulcerative colitis and 4 Crohn's disease data sets (Supplementary Table 1).

We also found that *TJP1* messenger RNA (mRNA) transcripts, which encode ZO-1, were markedly reduced in 5 of 6 of ulcerative colitis and 4 of 5 Crohn's disease data sets (Figure 1 and Supplementary Figure 1). Among these, 2 ulcerative colitis data sets included biopsy specimens from patients in remission, of which 1 (GSE59071) showed that ZO-1 down-regulation persisted, whereas the other (GSE128682) showed restoration of ZO-1 expression,

BASIC AND TRANSLATIONAL AT

* Authors share co-first authorship.

Abbreviations used in this paper: **4-OHT, 4-hydroxytamoxifen; DSS, dextran sodium sulfate; EdU, 5-ethynyl-2'-deoxyuridine; GSEA, gene set enrichment analysis; IBD, inflammatory bowel disease; mRNA, messenger RNA; MDCK, Madin-Darby canine kidney; NuMA, nuclear mitotic apparatus protein; qRT-PCR, quantitative reverse-transcription polymerase chain reaction; TNBS, trinitrobenzene sulfonic acid; WT, wild type; ZO-1, zonula occludens-1.**

Most current article

0016-5085/$36.00
https://doi.org/10.1053/j.gastro.2021.08.047

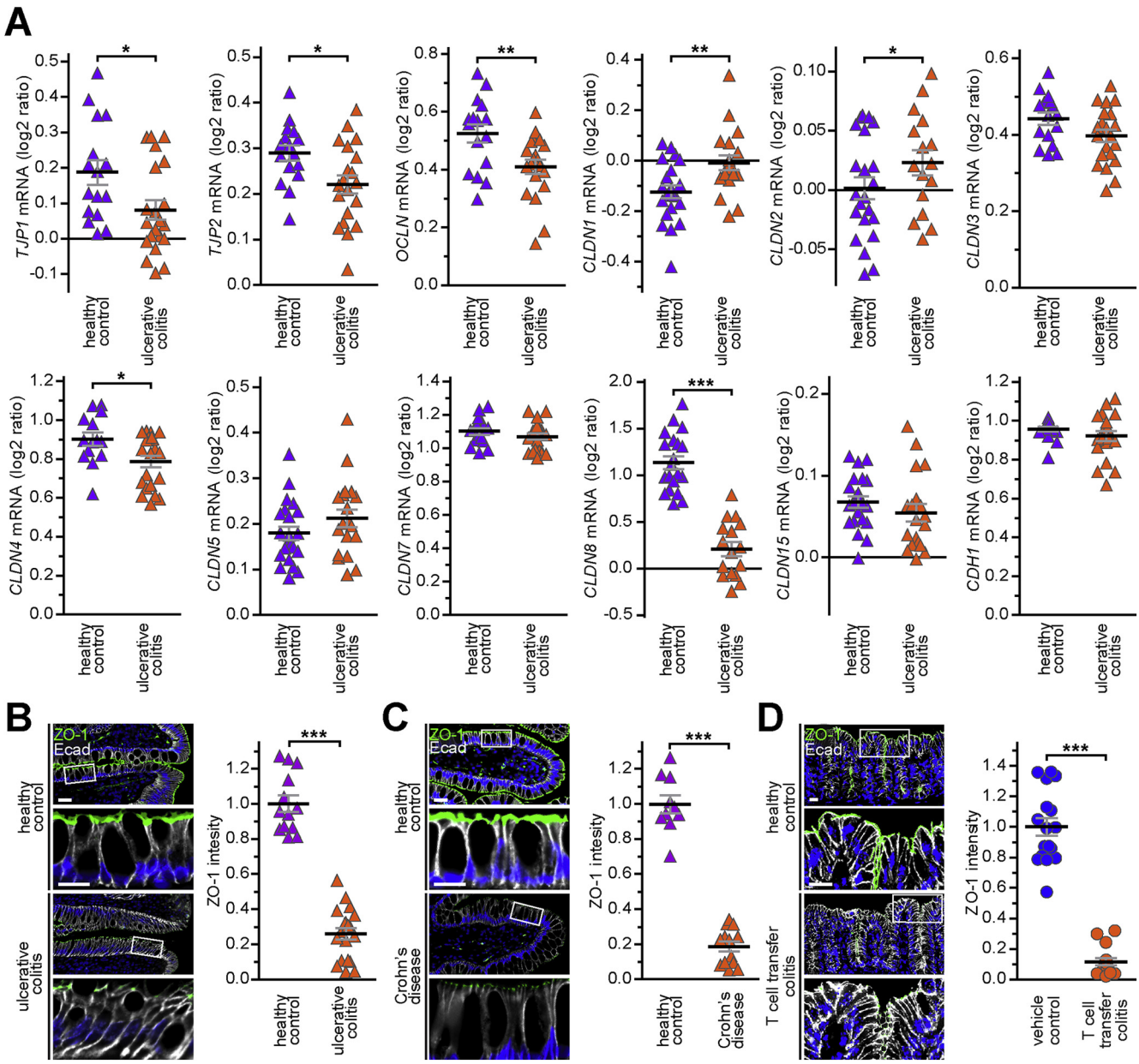

Figure 1. ZO-1 transcripts and protein are down-regulated in ulcerative colitis, Crohn's disease, and experimental immune-mediated IBD. (*A*) Relative transcript numbers for 11 tight junction proteins and E-cadherin are shown for 67 patients with ulcerative colitis (*orange triangles*) and 31 healthy control individuals (*purple triangles*) from data set GDS3268. (*B*, *C*) Quantitative immunofluorescence showing reduced ZO-1 (*green*) expression in colon biopsy specimens from 20 patients with ulcerative colitis (*orange triangles*) relative to 13 healthy control individuals (*purple triangles*) and ileal biopsy samples from 13 patients with Crohn's disease (*orange triangles*) relative to 10 healthy control individuals (*purple triangles*). (*D*) Quantitative immunofluorescence showing reduced ZO-1 expression (*green*) in colonic tissue from 15 mice with T cell adoptive transfer colitis (*orange circles*) relative to 17 littermate controls that did not receive T-cell transfer (*blue circles*). E-cadherin (*white*) and nuclei (*blue*) are shown for orientation in all micrographs. Scale bars: 20 μm or 10 μm (high magnification). Student *t* test. *$P <$ .05; **$P <$ .01; ***$P <$ .001. Ecad, E-cadherin.

during remission (Supplementary Figure 1). ZO-1 down-regulation may, therefore, be both a consequence of and contributor to disease.

The mRNA analyses are inconsistent with previous studies reporting that ZO-1 down-regulation in IBD is limited to sites of neutrophil transmigration.[5,7] We therefore assessed ZO-1 protein expression in IBD using a newly developed antibody validated for quantitative morphometry.[9] Colonic biopsy specimens from 18 patients with ulcerative colitis and 13 healthy control individuals as well as ileal biopsy specimens from 13 patients with Crohn's disease and 10 healthy control individuals were evaluated. ZO-1 protein expression was reduced 3.9 ± 0.03–fold in ulcerative colitis (Figure 1*B*) and 5.3 ± 0.03–fold in Crohn's disease (Figure 1*C*) and by 8.7 ± 0.06–fold in mice with immune-mediated T-cell transfer colitis (Figure 1*D*). ZO-1 transcription and protein expression are, therefore, significantly down-regulated in ulcerative colitis, Crohn's disease, and

immune-mediated experimental IBD. The T cell transfer colitis data further show that ZO-1 protein expression can be reduced in response to mucosal inflammation and, together with the human biopsy data, suggest a vicious cycle where ZO-1 down-regulation can also drive mucosal inflammation.

Intestinal Epithelial-Specific ZO-1 Knockout Does Not Cause Spontaneous Disease

Analysis of *Tjp1*-knockout mice is not possible because these mice are not viable.[10] We therefore generated intestinal epithelial–specific *Tjp1*-knockout mice (Figure 2*A*).[11] Expected numbers of pups expressing the villin-Cre transgene were born when $Tjp1^{f/f}$;vil-Cre^{Tg} (ZO-$1^{KO.IEC}$) mice were crossed to $Tjp1^{f/f}$ (WT) mice. Moreover, ZO-$1^{KO.IEC}$ mice grew and gained weight identically to their WT littermates (Supplementary Figure 2*A*). Despite the absence of *Tjp1* transcripts and ZO-1 protein (Figure 2*A*) within small intestinal and colonic epithelium, the transcription of other tight junction proteins was largely unaffected (Figure 2*B*). Moreover, no changes in tight junction protein transcription were detected in brain, lung, heart, liver, and kidney (Figure 2*B*). Finally, transmission electron microscopy, which is unbiased with respect to specific proteins, did not detect ultrastructural tight junction abnormalities in ZO-$1^{KO.IEC}$ mice (Figure 2*C*) but did confirm the presence of thickened cortical actin and disordered microvilli.[11]

Intestinal Epithelial ZO-1 Is Not Required for Mucosal Organization and Barrier Function

Conventional wisdom states that ZO-1 is essential for epithelial barrier function. We were therefore initially surprised at the absence of spontaneous disease in ZO-$1^{KO.IEC}$ mice. We first considered the possibility that some intestinal epithelial clones had escaped *Tjp1* deletion, as has been reported previously in some Cre-mediated knockouts,[12] but residual ZO-1 expression was not detected in small intestinal or colonic epithelium (Figure 2*D*).

We next assessed in vivo intestinal barrier function of ZO-$1^{KO.IEC}$ mice. We focused on leak and unrestricted pathway permeabilities using 4-kDa dextran (28-Å diameter) and 70-kDa dextran (120-Å diameter), respectively,[13,14] because ZO-1 knockdown increases leak pathway permeability in vitro.[15] Flux of 4-kDa dextran, but not 70-kDa dextran, was mildly increased in ZO-$1^{KO.IEC}$ mice (Figure 2*E*), consistent with increased leak pathway, that is macromolecular, permeability in vivo. Notably, the absence of increased 70-kDa dextran flux indicates the absence of mucosal damage and unrestricted pathway up-regulation.

Consistent with the absence of mucosal damage, transcripts for *Tnfsf2*, *Il1β*, *Il6*, and *Il17* were unaffected by intestinal epithelial ZO-1 knockout (Figure 2*F*). Furthermore, the expression and distribution of other epithelial transport and tight junction proteins were intact in ZO-$1^{KO.IEC}$ mice (Figure 2*G*). ZO-1 deletion did, however, reduce abundance of stem, enteroendocrine, Paneth, and tuft cells (Supplementary Figure 2*B* and *C*) as well as mRNA transcripts marking these cell types (Supplementary Figure 2*D*); *Muc2* transcripts and goblet cell numbers were similar in WT and ZO-$1^{KO.IEC}$. Thus, despite mildly increased leak pathway permeability, intestinal epithelial ZO-1 knockout has only minor effects on mucosal function and, most importantly, is insufficient to cause disease.

Intestinal Epithelial ZO-1 Is Critical for Efficient Mucosal Repair After Chemical Injury

It is common for phenotypes of mice lacking critical genes, such as *Rag1*, *Cldn2*, and *Ocln*,[4,13,16] to be revealed only after stress. ZO-$1^{KO.IEC}$ and WT littermates were therefore treated with 1% dextran sodium sulfate (DSS) for 6 days. This did not affect the weight of WT mice but did induce a robust proliferative response within the crypts and transit-amplifying zone, as indicated by increased 5-ethynyl-2′-deoxyuridine (EdU) incorporation (Figure 3*A* and *B*). In contrast, ZO-$1^{KO.IEC}$ mice displayed substantial weight loss and failed to significantly increase epithelial proliferation (Figure 3*A* and *B*).

To better understand their increased susceptibility, ZO-$1^{KO.IEC}$ mice and WT littermates were treated with 2% or 3% DSS (Figure 3*C* and *D*). Treatment with 2% DSS induced both greater weight loss and delayed recovery in ZO-$1^{KO.IEC}$, relative to WT, mice (Figure 3*C*). The more intense insult of 3% DSS resulted in similar degrees of initial injury and weight loss in ZO-$1^{KO.IEC}$ and WT mice, but ZO-$1^{KO.IEC}$ mice continued to show impaired recovery (Figure 3*D*). Moreover, the body weights of ZO-$1^{KO.IEC}$ mice never achieved those of DSS-treated WT littermates, even after prolonged periods of recovery. The effects of 1%, 2%, and 3% DSS on ZO-$1^{KO.IEC}$ and WT mice therefore show that epithelial ZO-1 deletion compromises mucosal repair.

Because it encompassed features of 1% and 3% DSS, 2% DSS was selected for further analysis. After 2% DSS treatment, the colons of ZO-$1^{KO.IEC}$ mice were shorter, thicker, and more erythematous, with greater areas of complete crypt loss and elevated histopathology scores, relative to WT mice (Figure 3*E* and *F*). Although 4-kDa dextran permeability increases were markedly greater in DSS-treated ZO-$1^{KO.IEC}$ mice relative to WT mice, this was due to flux across the unrestricted, rather than leak, pathway, because serum recovery of 70-kDa dextran was also far greater in ZO-$1^{KO.IEC}$, relative to WT, mice (Figure 3*G*), and both dextrans are able to traverse the unrestricted pathway (Figure 2*E*).[14] This contrasts with the specific leak pathway up-regulation indicated by the increased flux of 4-kDa, not 70-kDa, dextran in unstressed ZO-$1^{KO.IEC}$ mice (Figure 2*E*). As with 1% DSS, 2% DSS failed to induce increases in DNA synthesis (Figure 3*H*) or the MKI67 (Ki-67) proliferative index (Figure 3*I*) in ZO-$1^{KO.IEC}$ mice. Moreover, mucosal inflammatory responses, measured as cytokines (Figure 3*J*) as well as infiltration of $CD3^+$ T cells (Figure 3K) and $CD68^+$ mononuclear cells, such as macrophages (Figure 3*L*), were far greater in ZO-$1^{KO.IEC}$ mice.

Although the data show that ZO-1 is critical to mucosal healing and that ZO-1 loss leads to defective activation of repair processes, they do not fully exclude the possibility that ZO-1 also limits sensitivity to DSS-induced injury. To address this, we exposed mice to trinitrobenzene sulfonic acid (TNBS), which induces damage via a different process

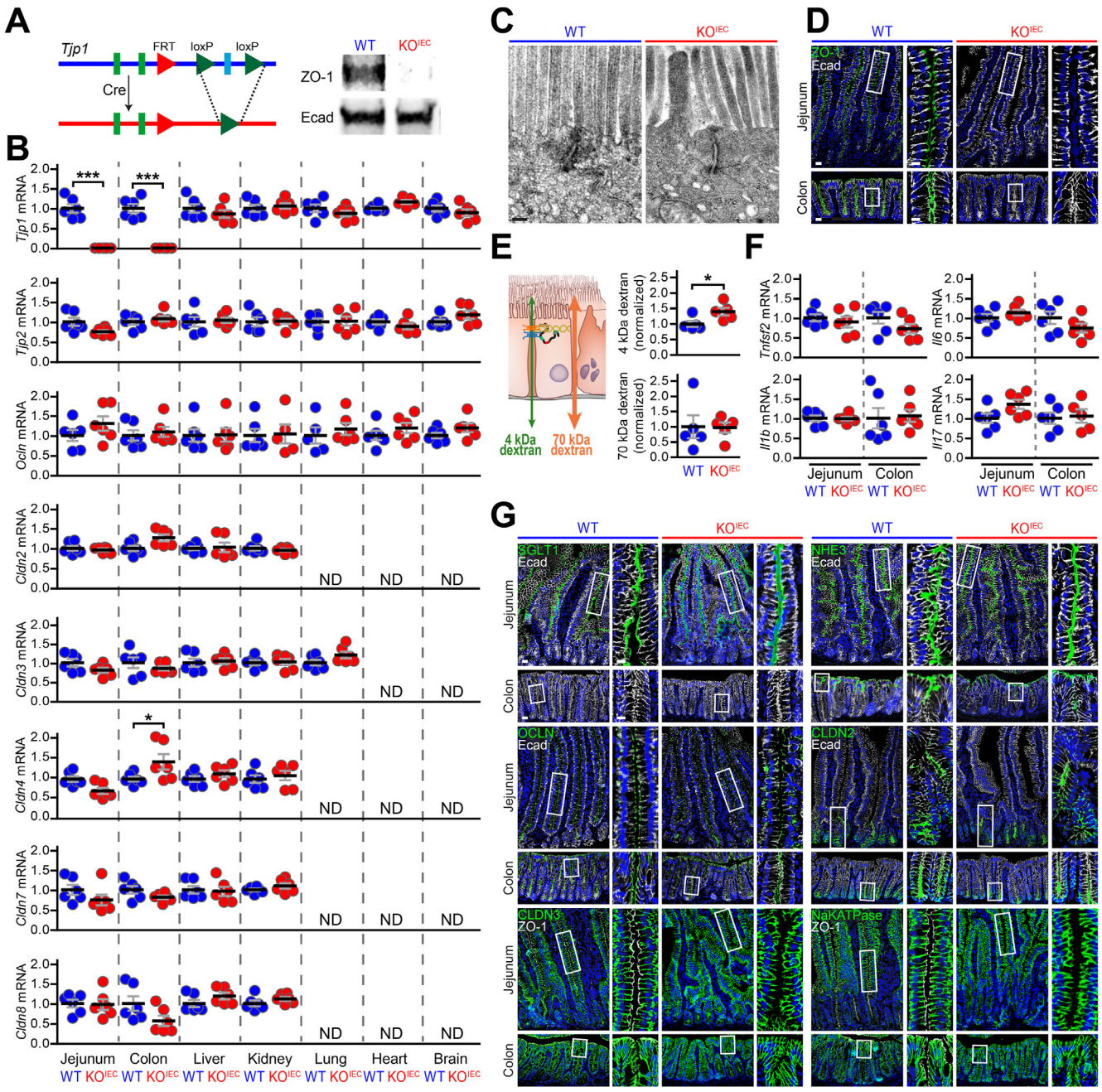

Figure 2. ZO-1 deletion in intestinal epithelial cells results in only mild increases in paracellular leak pathway permeability. (*A*) Floxed allele before and after Cre-mediated recombination and Western blots of isolated colonic epithelial cells from *Tjp1*$^{f/f}$ (WT) and *Tjp1*$^{f/f}$;vil-Cre^{Tg} (ZO-1$^{KO.IEC}$) mice. (*B*) qRT-PCR of transcripts from jejunal epithelial cells, colonic epithelial cells, kidney, lung, heart, and brain of ZO-1$^{KO.IEC}$ (*red circles*) and WT (*blue circles*) mice. Only *Tjp1* (ZO-1) transcripts and, in the colon, *Cldn4* (claudin-4) transcripts were affected. n = 6 per group. (*C*) Representative transmission electron micrographs of jejunal epithelium from ZO-1$^{KO.IEC}$ and WT mice. No differences in tight junction morphology were detected. (*D*) Representative micrographs confirming loss of ZO-1 (*green*) expression in jejunum and colon of ZO-1$^{KO.IEC}$ mice. (*E*) Permeability of the tight junction–dependent leak and tight junction–independent unrestricted pathway probes 4-kDa and 70-kDa dextran, respectively, showing that ZO-1 deletion causes a small, but significant, increase in leak pathway permeability without affecting the unrestricted pathway. n = 5 per group. (*F*) qRT-PCR of mucosal transcripts shows that ZO-1 deletion does not alter cytokine expression in jejunum or colon. n = 6 per group. (*G*) Representative immunofluorescence of indicated transport and tight junction proteins (*green*) in jejunum and colon of ZO-1$^{KO.IEC}$ and WT mice. E-cadherin (*white*) and nuclei (*blue*) are shown for orientation in all micrographs. Scale bars: 20 μm, 10 μm (high magnification), or 200 nm (electron micrographs). Student *t* test. *$P < .05$; ***$P < .001$. KO, knockout; ND, not detected.

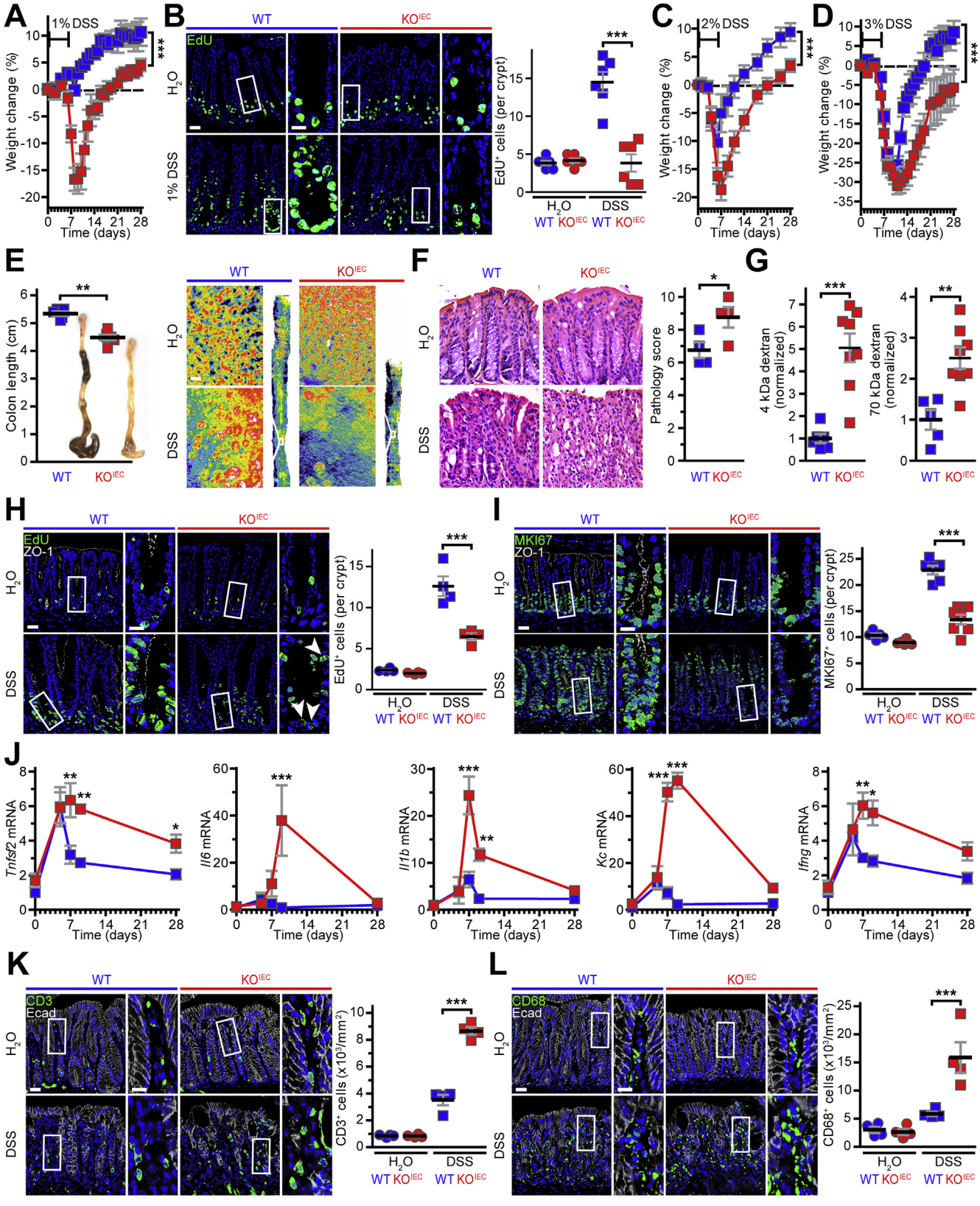
A
1% DSS
Weight change (%)
Time (days)
B
WT
KO^IEC
EdU
H2O
1% DSS
EdU+ cells (per crypt)
C
2% DSS
D
3% DSS
E
Colon length (cm)
F
Pathology score
G
4 kDa dextran (normalized)
70 kDa dextran (normalized)
H
EdU
ZO-1
I
MKI67
ZO-1
MKI67+ cells (per crypt)
J
Tnfsf2 mRNA
Il6 mRNA
Il1b mRNA
Kc mRNA
Ifng mRNA
K
CD3
Ecad
CD3+ cells (x10³/mm²)
L
CD68
CD68+ cells (x10³/mm²)

than DSS. Weight loss, clinical scores, unrestricted pathway permeability increases, pathology scores, and cytokine production were all greater in ZO-1$^{KO.IEC}$, relative to WT, mice, and epithelial proliferative responses were markedly diminished (Supplementary Figure 3). These similar effects of ZO-1 deletion in 2 distinct chemically-induced colitis models that cause damage by different processes but share mechanisms of repair indicate that disruption of repair is the primary means by which ZO-1 loss enhances colitis severity.

Intestinal Epithelial ZO-1 Promotes Mucosal Healing After Immune-Mediated Injury

DSS and TNBS cause severe colitis but are not representative of immune-mediated human disease. As a simple model of immune-mediated mucosal damage, disseminated T-cell activation and cytokine storm were induced by treating mice with anti-CD3. This results in acute cytokine-driven diarrhea, without epithelial damage, that resolves by 5 hours after anti-CD3 administration.[17] After a 12–18-hour asymptomatic interval, WT mice develop severe small intestinal mucosal damage and inflammatory diarrhea that remits by day 4. Despite similar damage 2 days after anti-CD3 administration (Figure 4*A*), activation of both epithelial proliferation and repair were defective (Figure 4*B* and Supplementary Figure 4*A*) and epithelial apoptosis was increased (Supplementary Figure 4*B*) in ZO-1$^{KO.IEC}$ relative to WT mice. This supports the conclusion, based on impaired recovery after 3% DSS treatment, that repair is the primary abnormality in ZO-1-deficient epithelial cells. Consistent with this, histologic damage as well as *Il6*, *Ifng*, and *Il1b* transcripts were greater in ZO-1$^{KO.IEC}$ mice than WT mice (Supplementary Figure 4*C*). ZO-1 is, therefore, required for effective epithelial repair after either immune-mediated or chemically induced mucosal damage.

To better understand the mechanisms responsible for defective repair responses in the absence of epithelial ZO-1 expression, jejunal epithelial cells were harvested from ZO-1$^{KO.IEC}$ and WT mice before as well as 2 and 4 days after anti-CD3 treatment. Gene set enrichment analysis (GSEA) of RNA-sequencing data from isolated intestinal epithelium showed that, in the absence of exogenous stress, Wnt–β-catenin signaling was reduced in ZO-1$^{KO.IEC}$ relative to WT mice (Figure 4*C*). These differences were confirmed by quantitative reverse-transcription polymerase chain reaction (qRT-PCR) analysis showing reduced expression of *Wnt3*, *Lgr5*, *Olfm4*, *Ascl2*, *Bmi1*, *Hopx*, and *Notch1* transcripts in jejunal epithelial from ZO-1$^{KO.IEC}$, relative to WT, mice (Supplementary Figure 2*D*).

Comparisons between ZO-1$^{KO.IEC}$ and WT GSEA data before, 2 days after, and 4 days after anti-CD3 administration showed that activation of Wnt–β-catenin signaling, as well as mitotic spindle, G2/M checkpoint, DNA repair, oxidative phosphorylation, and glycolysis pathways, was defective in ZO-1$^{KO.IEC}$ mice at 2 days after anti-CD3 treatment (Figure 4*C*). These differences were no longer present at day 4, primarily because the pathways were down-regulated in WT mice (Figure 4*D*); only minor activation was detected in ZO-1$^{KO.IEC}$ jejunal epithelial cells, even 4 days after anti-CD3 treatment. These data indicate that ZO-1 loss both delays and attenuates activation of repair responses.

ZO-1 Knockout Causes a Cell-Intrinsic Proliferative Defect

We turned to in vitro colonoid culture and 4-hydroxytamoxifen (4-OHT)–inducible Cre to better characterize the proliferative defect in ZO-1–deficient epithelia. Colonic crypt cells from *Tjp1*$^{f/f}$ and *Tjp1*$^{f/f}$;vil-Cre-ERT2^{Tg} mice grew and proliferated indistinguishably in the absence of 4-OHT (Figure 5*A*). Treatment with 4-OHT extinguished ZO-1 expression in *Tjp1*$^{f/f}$;vil-Cre-ERT2^{Tg} colonoids (Figure 5*B*) and markedly reduced growth and proliferation as measured by cross-sectional area and bud, or crypt-like domain, numbers, respectively (Figure 5*C* and *D*). In contrast, 4-OHT did not affect *Tjp1*$^{f/f}$ colonoids. Similar experiments comparing *Tjp1*$^{f/f}$ and *Tjp1*$^{f/f}$;vil-Cre^{Tg} colonoids yielded comparable results (Supplementary Figure 5*A*).

We attempted to rescue Wnt signaling and growth in ZO-1$^{KO.IEC}$ colonoids using the GSK3 inhibitor CHIR99021. This significantly increased the growth and proliferation of *Tjp1*$^{f/f}$;vil-Cre-ERT2^{Tg} colonoids (without 4-OHT) and 4-OHT–treated *Tjp1*$^{f/f}$ colonoids but failed to stimulate 4-OHT–treated *Tjp1*$^{f/f}$;vil-Cre-ERT2^{Tg} colonoids (Figure 5*E*–*G*). DNA synthesis (Figure 5*H* and *I*) and participation in the cell cycle (Figure 5*J* and *K*) were also defective in

Figure 3. Mucosal repair is defective in ZO-1$^{KO.IEC}$ mice. (*A*) ZO-1$^{KO.IEC}$ (*red squares*) and WT (*blue squares*) mice were treated with 1% DSS for 6 days and then returned to normal water. Weight curves are shown. n = 4 or 5 per group. (*B*) EdU (*green*) was administered 2 hours before mice were killed. Treatment with 1% DSS markedly increased numbers of proliferating cells in WT, but not ZO-1$^{KO.IEC}$, mice. n = 4 or 5 per group. (*C, D*) Weight curves of ZO-1$^{KO.IEC}$ and WT mice treated with 2% or 3% DSS for 6 days and allowed to recover. n = 6 or 7 per group. (*E*) Colonic shortening after 2% DSS treatment is significantly greater in ZO-1$^{KO.IEC}$ relative to WT mice. Representative pseudocolor images of methylene blue–stained colons at low and high magnification show that crypts are completely lost in ZO-1$^{KO.IEC}$ but partially preserved in WT mice. n = 5 or 6 per group. (*F*) Representative images and histopathology scores of ZO-1$^{KO.IEC}$ and WT mice without DSS exposure (H_2O) or after 6 days of 2% DSS treatment and 1 day of recovery (DSS). n = 4 per group. (*G*) Permeability of both 4-kDa dextran and 70-kDa dextran is dramatically increased in 2% DSS–treated ZO-1$^{KO.IEC}$ relative to WT mice. This indicates greater mucosal damage and unrestricted pathway permeability rather than increased tight junction leak pathway permeability. n = 6–8 per group. (*H, I*) EdU and MKI67 (*green*) stains show similar numbers of proliferating cells in ZO-1$^{KO.IEC}$ and WT mice at baseline. However, only WT mice are able to significantly increase proliferation in response to 2% DSS. ZO-1 (*white*) and nuclei (*blue*) are shown for orientation. n = 4–6 per group. (*J*) qRT-PCR of mucosal transcripts before and after 6 days of 2% DSS treatment and during recovery show both increased and prolonged cytokine elevation in ZO-1$^{KO.IEC}$, relative to WT, mice. n = 5 per group. (*K, L*) Infiltration of CD3$^+$ T cells and CD68$^+$ macrophages (*green*) is markedly greater in 2% DSS–treated ZO-1$^{KO.IEC}$, relative to WT, mice. E-cadherin (Ecad, *white*) and nuclei (*blue*) are shown for orientation. n = 4 per group. Scale bars: 20 μm, 10 μm (high magnification), and 500 μm (pseudocolor gross image). Student *t* test (*A*–*G*) and analysis of variance with Bonferroni correction (*H*–*L*). *$P < .05$; **$P < .01$; ***$P < .001$.

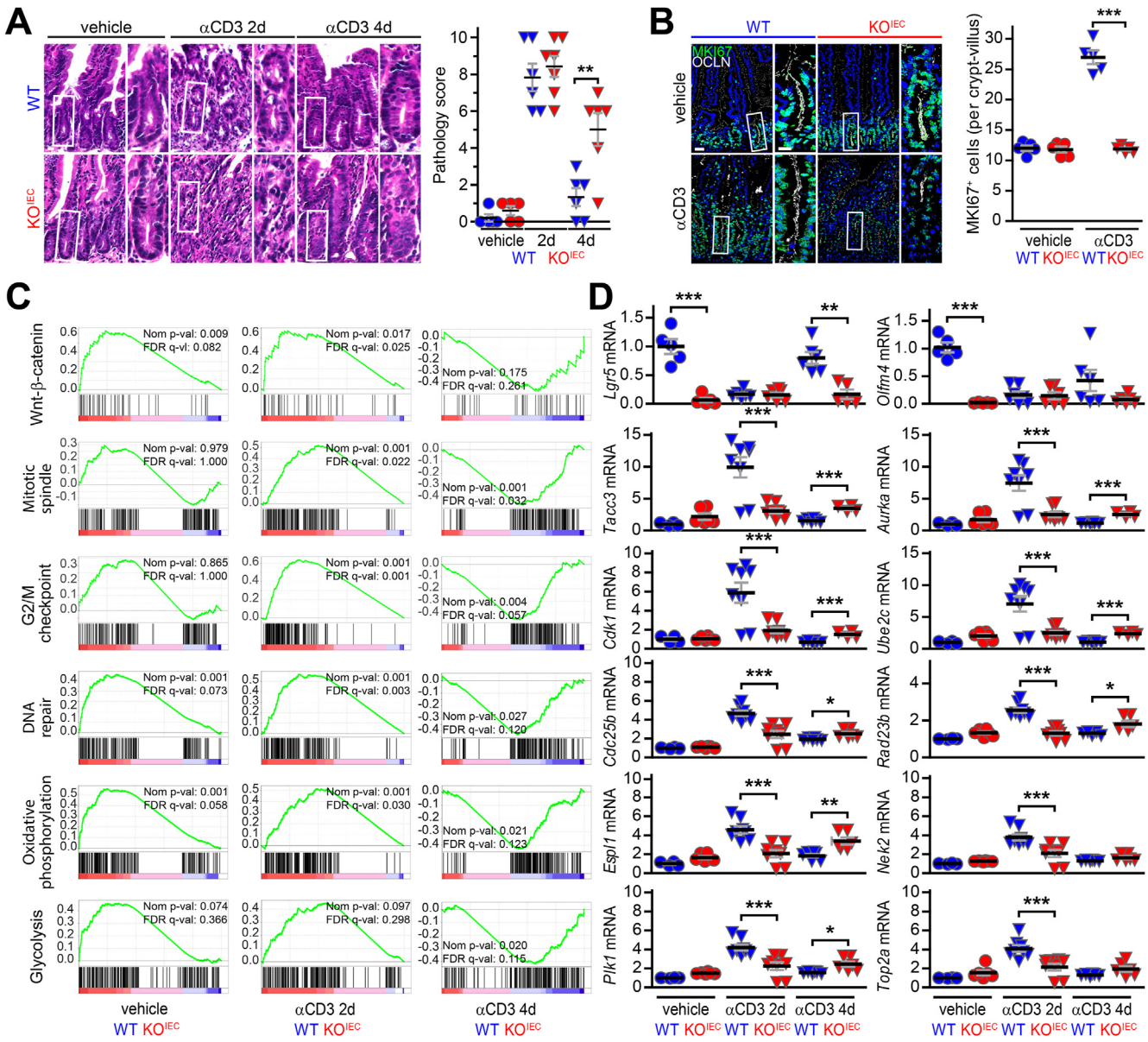

Figure 4. Epithelial ZO-1 deletion delays and attenuates transcriptional responses to T-cell activation–induced mucosal injury. (*A*) Representative images and histopathology scores of jejunum from ZO-1$^{KO.IEC}$ (*red*) and WT mice (*blue*) before, 2 days after, and 4 days after anti-CD3 treatment. Despite similar injury scores at 2 days, subsequent repair (at 4 days) was relatively ineffective in ZO-1$^{KO.IEC}$ mice. n = 5–7 per group. (*B*) MKI67 (*green*) immunostains show similar numbers of proliferating cells in jejunal mucosae of ZO-1$^{KO.IEC}$ and WT mice at baseline. However, only WT mice display significantly increased proliferation at 2 days after anti-CD3 treatment. n = 5 per group. (*C*) GSEA of RNA-sequencing data from jejunal epithelia. Comparisons of ZO-1$^{KO.IEC}$ and WT transcripts before and 2 and 4 days after anti-CD3 treatment are shown. Activation of repair pathways is markedly deficient in ZO-1$^{KO.IEC}$ mice. The green line in each graph shows, by rank, transcripts from the indicated pathway with increased (positive values) or reduced (negative values) expression. Vertical black lines indicate the location of individual genes on the green curves. Normalized *P* values and false discovery rate *Q* values are shown on each graph. (*D*) qRT-PCR of representative transcripts before, 2 days after, and 4 days after anti-CD3 treatment confirm defective transcriptional activation in ZO-1$^{KO.IEC}$ jejunal epithelia. n = 4–8 per group. Scale bars: 20 μm or 10 μm (high magnification). Analysis of variance with Bonferroni correction. **P* < .05; ***P* < .01; ****P* < .001. 2d, 2 days; 4d, 4 days; FDR, false discovery rate; Norm, normalized.

4-OHT–treated *Tjp1*$^{f/f}$;vil-Cre-ERT2^{Tg} colonoids. Results using *Tjp1*$^{f/f}$ and *Tjp1*$^{f/f}$;vil-Cre colonoids (Supplementary Figure 5*A*) also showed reduced expression of the stem and transit-amplifying cell markers *Lgr5, Lrig1, Cdk2,* and *Pcna* in ZO-1$^{KO.IEC}$, relative to WT, colonoids (Supplementary Figure 5*B*). Finally, in vitro analyses confirmed that ZO-1 deletion was responsible for the observed defects because both basal and CHIR99021-augmented proliferation were rescued by transgenic mRFP1-ZO-1 expression in colonoids isolated from *Tjp1*$^{f/f}$;vil-Cre^{Tg};vil-Cre-mRFP1-ZO1 mice (Supplementary Figure 5*C*). ZO-1 deficiency therefore causes an epithelial-intrinsic proliferative deficiency that is insensitive to GSK3 inhibition and results in reduced numbers of stem and transit-amplifying cells.

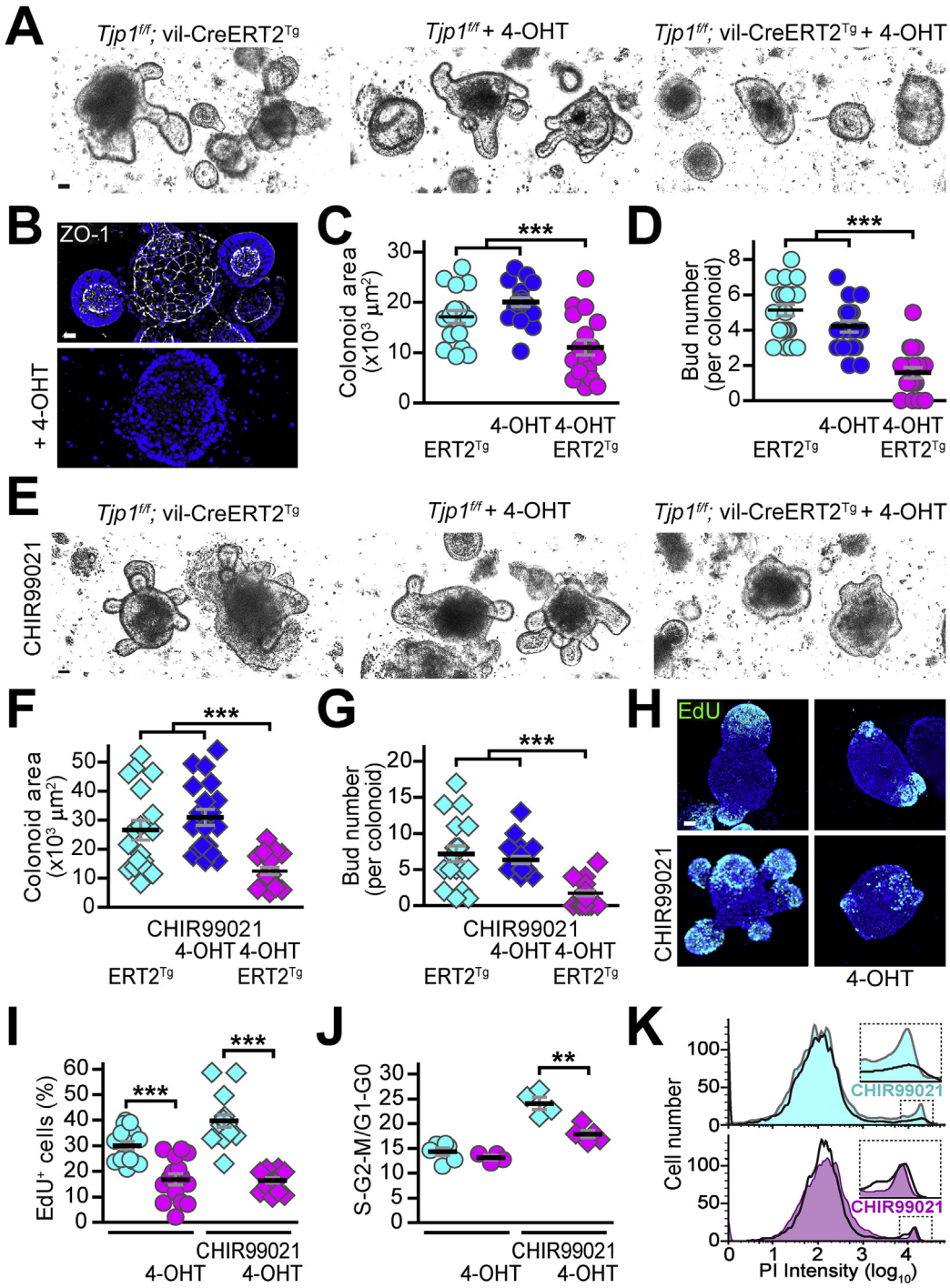

Figure 5. ZO-1 deletion compromises epithelial proliferation in colonoid cultures. (*A–C*) Colonic epithelial stem cells were harvested from *Tjp1*$^{f/f}$;vil-CreERT2^{Tg} and *Tjp1*$^{f/f}$ mice. Two days after passage, 1 μmol/L 4-OHT was added to the media as indicated; 4-OHT had no effect on *Tjp1*$^{f/f}$ colonoids but markedly reduced growth of *Tjp1*$^{f/f}$;vil-CreERT2^{Tg} colonoids. Representative images are shown. n = 18–20 per group. (*D*) Treatment with 4-OHT effectively eliminated ZO-1 (*white*) expression. Nuclei (*blue*) are shown for reference. (*E–G*) Stem cells harvested from *Tjp1*$^{f/f}$;vil-CreERT2^{Tg} and *Tjp1*$^{f/f}$ mice were treated with 4-OHT, as indicated, and the GSK3 inhibitor CHIR99021 (5 μmol/L). CHIR99021 enhanced growth and budding within *Tjp1*$^{f/f}$;vil-CreERT2^{Tg} and 4-OHT–treated *Tjp1*$^{f/f}$ colonoids but was ineffective in 4-OHT–treated *Tjp1*$^{f/f}$;vil-CreERT2^{Tg} colonoids. Representative images are shown. n = 18–22 per group. (*H*, *I*) CHIR99021 enhanced EdU incorporation within *Tjp1*$^{f/f}$ vil-CreERT2^{Tg} and 4-OHT–treated *Tjp1*$^{f/f}$ colonoids but was ineffective in 4-OHT–treated *Tjp1*$^{f/f}$;vil-CreERT2^{Tg} colonoids. n = 18–20 per group. (*J*, *K*) CHIR99021 increased the fraction of cells in the S-G2-M phases of the cell cycle within *Tjp1*$^{f/f}$;vil-CreERT2^{Tg} and 4-OHT–treated *Tjp1*$^{f/f}$ colonoids but was ineffective in 4-OHT–treated *Tjp1*$^{f/f}$;vil-CreERT2^{Tg} colonoids. Representative histograms of flow cytometric data from propidium iodide–stained cells without (*dark lines*) or after (*grey lines*) CHIR99021 treatment are shown. n = 4–6 per group. Scale bars: 20 μm. Analysis of variance with Bonferroni correction. $^{**}P < .01$; $^{***}P < .001$. PI, propidium iodide.

ZO-1 Deletion Leads Failure of Mitotic Spindle Orientation, Abortive Proliferation, and Apoptosis

We hypothesized that the relative health of unstressed ZO-1$^{KO.IEC}$ mice might reflect the ability of ZO-1–deficient epithelial cells to proliferate at near-normal basal levels despite being incapable of up-regulating proliferation in response to injury. To assess this, EdU incorporation was monitored after 2 and 24 hours of continuous labeling. As expected, the number of labeled WT cells nearly doubled over this interval (Figure 6*A*). In contrast, there was no

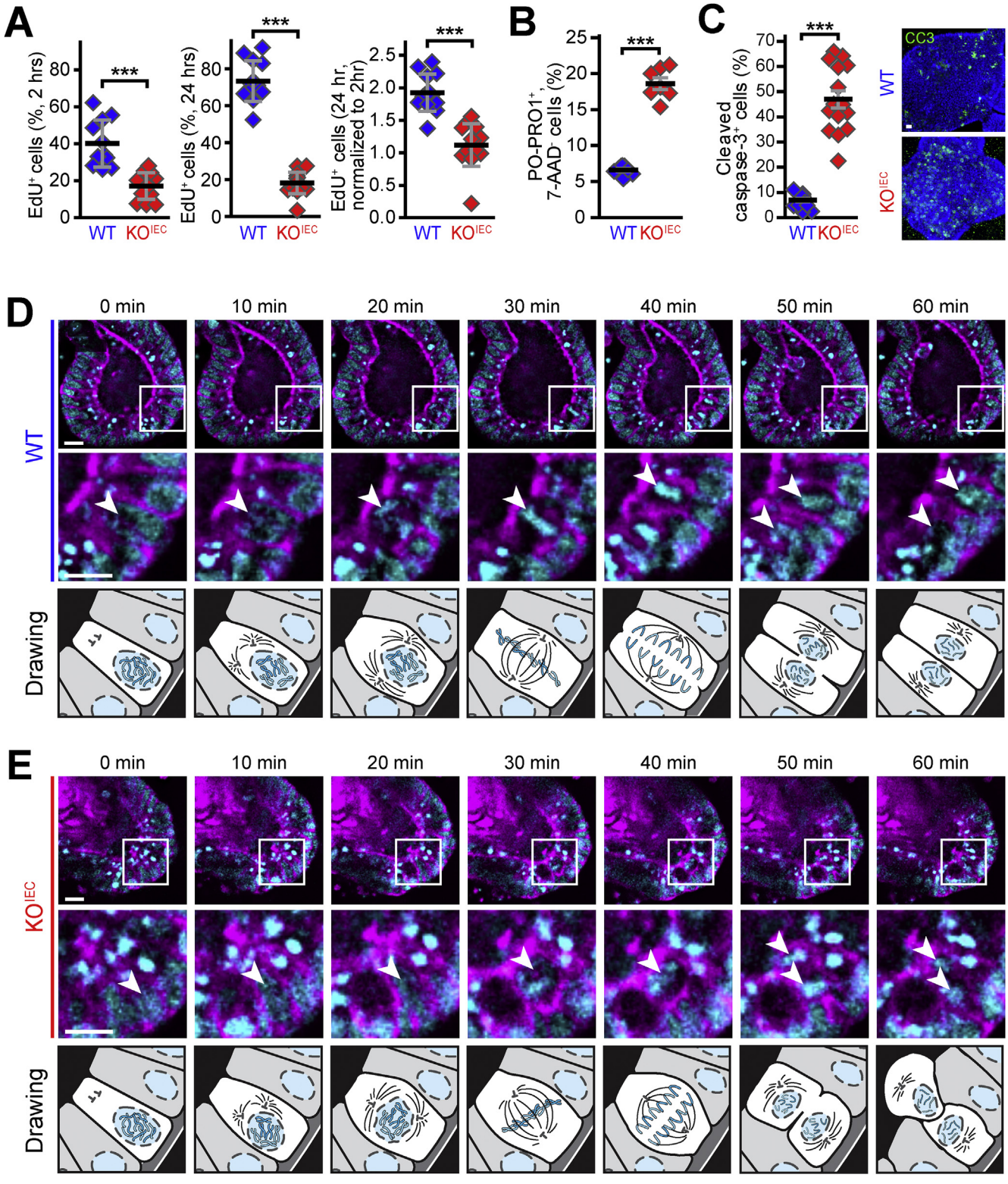

significant change in the number of EdU-labeled ZO-1$^{KO.IEC}$ cells (Figure 6*A*). Although less than half as many ZO-1$^{KO.IEC}$ cells, relative to WT, were labeled at 2 hours, the absence of any increase suggests that, in addition to a reduced proliferation rate, ZO-1$^{KO.IEC}$ cells were unable to progress and successfully complete the process of cell division. This defect is referred to as *failure of mitotic progression* and typically results in mitotic catastrophe, a form of apoptosis.[18] Consistent with this, numbers of PO-PRO1–positive, 7-amino-actinomycin D–negative cells, that is, apoptotic cells, were nearly 4-fold greater in ZO-1$^{KO.IEC}$, relative to WT, colonoids (Figure 6*B*). Apoptosis induced by mitotic catastrophe often involves caspase-3 activation; the number of cleaved caspase-3^{+} cells was more than 4-fold greater in ZO-1$^{KO.IEC}$, relative to WT, colonoids (Figure 6*C*).

The GSEA showing delayed and attenuated activation of mitotic spindle and G2/M checkpoint pathways in ZO-1$^{KO.IEC}$ suggested that ZO-1 might be required for mitotic spindle orientation. qRT-PCR of individual mRNA species confirmed delayed and attenuated transcription of centrosome and mitotic spindle components, including *Tacc3*, *Aurka*, *Espl1*, *Nek2*, and *Plk1*, as well as proteins involved in chromatid separation, identification of DNA damage sites, or mitotic progression, for example, *Top2a*, *Rad23b*, *Cdk1*, *Ube2c*, and *Cdc25b* (Figure 4*D*). We therefore considered the possibility that mitotic catastrophe could contribute to the failure of EdU^{+} ZO-1$^{KO.IEC}$ cells to accumulate over 24 hours of labeling.

To identify the stage at which cell division failed in ZO-1$^{KO.IEC}$ cells, colonoids expressing fluorescent-tagged β-actin and histone 2B were imaged during cell division. Mitotic events were easily recognized by apical nuclear displacement within the epithelial monolayer (Figure 6*D*). As the process matured, chromosomes segregated and WT cells oriented the spindle pole such that a line connecting the 2 centrioles was parallel to the basal surface of the monolayer. This was followed by formation of the metaphase plate and cell division in a plane perpendicular to the apical plasma membrane. The 2 daughter cells maintained contact with the basement membrane and their nuclei and then returned to the monolayer.

Initial phases of mitosis in ZO-1$^{KO.IEC}$ colonoids were similar to WT. Mitotic spindle orientation was, however, nearly always defective in ZO-1$^{KO.IEC}$ colonoids (Figure 6*E*). Mitotic spindles failed to orient correctly, with the metaphase plate nearly perpendicular to the apical cell membrane, and, when cytokinesis completed, only 1 daughter nucleus returned to the monolayer (Figure 6*E*). The second daughter cell lost contact with the basement membrane, and the nucleus failed to return to the monolayer. This led to an accumulation of bright, compact nuclei consistent with the condensation that occurs during apoptosis (Figure 6*E*). The data therefore indicate that mitotic catastrophe and apoptosis occur in ZO-1$^{KO.IEC}$ cells because of defective spindle orientation. In sum, this abortive proliferative process prevents net cell number increases.

ZO-1 Associates With the Centriole and Mitotic Spindle and Is Required for Mitotic Spindle Orientation In Vivo

ZO-1 has been localized to the nucleus of actively proliferating cells[19] and is known to associate closely or bind directly to actomyosin, microtubules, and associated proteins,[20] some of which are present at the mitotic spindle. To evaluate the potential association of ZO-1 with the mitotic apparatus during cell division, colonoids were prepared from transgenic mice that express mRFP-ZO-1 within the intestinal epithelium.[21] Cytoplasmic foci of ZO-1 were frequently identified at the poles of dividing cells, although these were difficult to recognize in individual z-sections because nuclei, spindles, and ZO-1 were typically in separate planes, and colonoids actively move during 3-dimensional culture. ZO-1 spots at spindle pole processes were, however, easily detected using 3-dimensional reconstructions (Figure 7*A*). These images showed the appearance of 2 bright cytoplasmic ZO-1 foci as the nucleus of the dividing cell moved apically. One bright focus of ZO-1 remained associated with each newly formed daughter nucleus as they moved back into the monolayer. ZO-1 therefore associates transiently with the mitotic apparatus during epithelial cell division.

We have previously reported that, in transgenic mice, mRFP-ZO-1 is present both at tight junctions and in bright subapical foci.[21] We considered the hypothesis that these might represent interphase centrioles, which are located within the subapical cytoplasm in the same z-plane as tight junction–associated ZO-1.[22] To avoid potential artifacts due to fusion protein overexpression, intestinal epithelial cytopreps from WT (not *Tjp1*$^{f/f}$) mice were fixed using –20°C methanol (to precipitate proteins in place); this allowed

Figure 6. ZO-1 is required for mitotic spindle orientation and productive mitosis. (*A*) ZO-1$^{KO.IEC}$ and WT colonoids were treated with CHIR99021 and harvested 2 hours and 24 hours after EdU addition. Numbers of labeled cells increased markedly over this interval in WT but not ZO-1$^{KO.IEC}$ colonoids. n = 10–13 per group. (*B*, *C*) Numbers of PO-PRO1^{+}, 7-AAD^{-}, and cleaved caspase-3^{+} apoptotic cells are much greater in CHIR99021-treated ZO-1$^{KO.IEC}$, relative to WT, colonoids. n = 5–9 per group. (*D*, *E*) Colonoids were grown from WT and ZO-1$^{KO.IEC}$ mice expressing EGFP-β-actin (*magenta*) and H2B-mCherry (*cyan*). Images were collected at 10-minute intervals. The mitotic spindle (*arrows*) is well oriented in WT (30 minutes) but not ZO-1$^{KO.IEC}$ (40 minutes) colonoids. The chromosomes separate according to the mitotic spindle planes 10 minutes later (*arrows*). This results in production of 2 daughter cells, both in contact with the basal matrix material, whose nuclei returned to the normal interphase position in WT colonoids. In contrast, only 1 daughter cell maintained basal contact in ZO-1$^{KO.IEC}$; the second daughter cell was shed into the lumen. Mitotic events representative of the majority of cell divisions for each genotype are shown. The drawings below each set of images are presented to help simplify the interpretation of the micrographs. Scale bars: 10 μm. Student *t* test. *$P < .05$; ***$P < .001$.

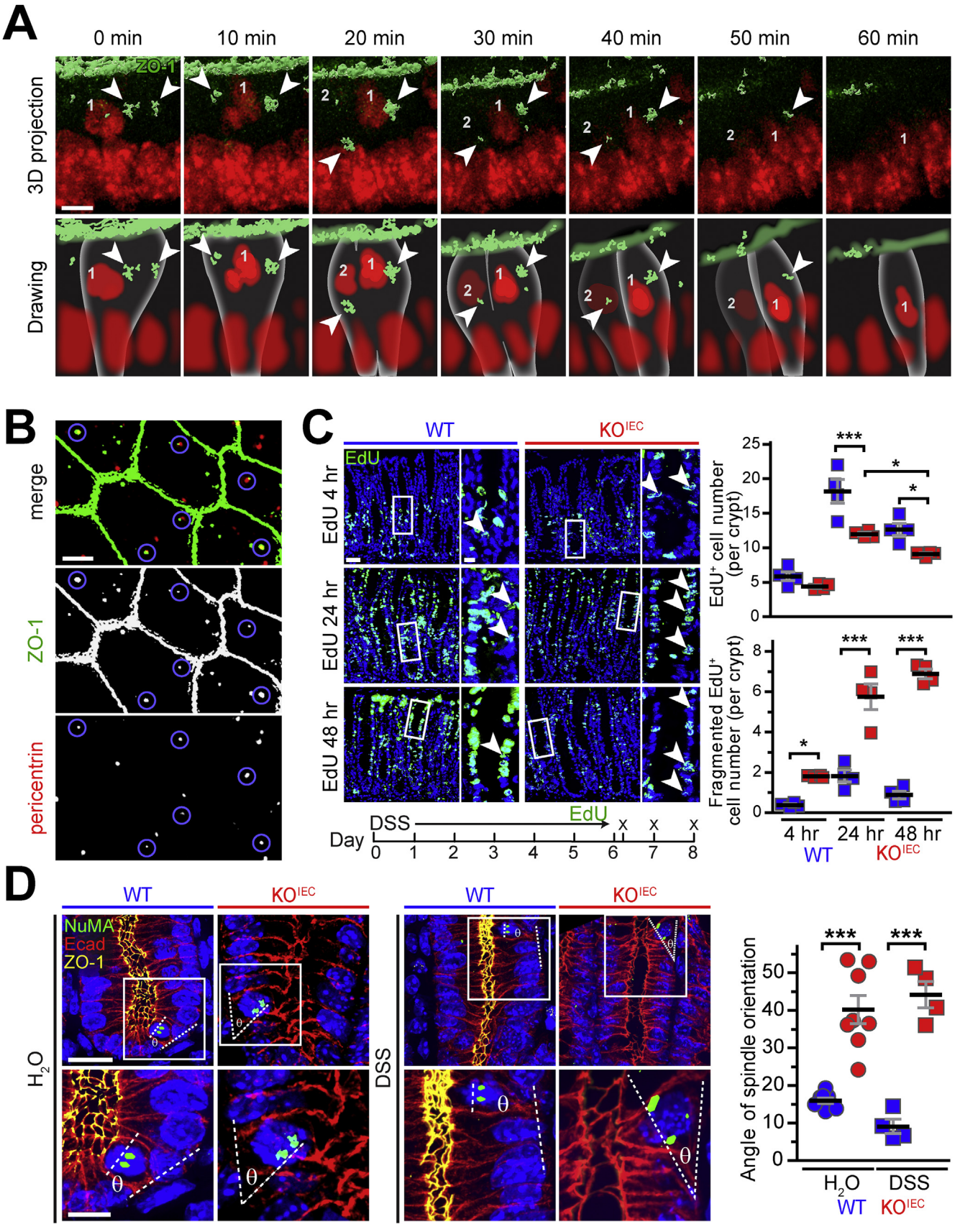
A
0 min
10 min
20 min
30 min
40 min
50 min
60 min
3D projection
Drawing
ZO-1
B
merge
ZO-1
pericentrin
C
WT
KO^IEC
EdU
EdU 4 hr
EdU 24 hr
EdU 48 hr
DSS
Day
EdU
0 1 2 3 4 5 6 7 8
EdU+ cell number (per crypt)
Fragmented EdU+ cell number (per crypt)
4 hr 24 hr 48 hr
WT KO^IEC
D
WT
KO^IEC
NuMA
Ecad
ZO-1
H2O
DSS
θ
Angle of spindle orientation
H2O DSS
WT KO^IEC

immunodetection of ZO-1 foci within the apical cytoplasm (Figure 7*B*). These ZO-1 foci colocalized with pericentrin (Figure 7*B*). Thus, in addition to associating with mitotic spindle poles during cell division, ZO-1 is present at interphase centrioles.

ZO-1 localization at mitotic spindles provides a potential explanation for the failure of ZO-1$^{KO.IEC}$ mice to recover fully from mucosal injury. To determine whether abortive proliferation occurred in vivo, WT and ZO-1$^{KO.IEC}$ mice were injected with EdU immediately after ending 6 days of treatment with 2% DSS. Mice were killed 4 hours, 24 hours, and 48 hours later. As expected, the numbers of EdU-positive colonocyte nuclei increased progressively in WT mice, with labeled nuclei throughout the expanded transit-amplifying zone at 24 hours (Figure 7*C*). By 48 hours, the numbers of labeled nuclei decreased, and those that remained were concentrated within the upper one third of the crypt, consistent with normal turnover (Figure 7*B*). Numbers of EdU-positive nuclei also increased between 4 hours and 24 hours in ZO-1 KO^{IEC} mice, albeit less robustly than in WT mice (Figure 7*C*). However, labeled nuclei were scattered throughout the crypt and did not move to the surface as a wave in ZO-1 KO^{IEC} mice (Figure 7*C*). On closer examination, it was apparent that many of the labeled nuclei in ZO-1 KO^{IEC} colons were fragmented, characteristic of apoptosis. The number of fragmented nuclei in ZO-1 KO^{IEC} mice increased dramatically between 4 hours and 24 hours and remained elevated at 48 hours; this did not occur in WT mice (Figure 7*C*). Thus, consistent with the in vitro observations, the in vivo data indicate that ZO-1 deletion results in abortive proliferation and apoptosis.

Finally, we asked if, similar to in vitro colonoid culture, spindle orientation was defective in ZO-1–deficient epithelia in vivo. To assess this, sections from control and DSS-treated WT and ZO-1$^{KO.IEC}$ mice were stained for ZO-1 and the nuclear mitotic apparatus protein (NuMA), an essential component of centrosomes.[23] Spindle orientation was assessed by drawing a straight line connecting the NuMA-containing spindle poles and a second line along the basement membrane at that site. These lines should be nearly parallel, with an angle between them of less than approximately 20° if the spindle is correctly oriented.[11] This was the case in WT epithelia, both without and after DSS treatment (Figure 7*D*). In contrast, spindle orientation was frequently defective in ZO-1$^{KO.IEC}$ epithelia (Figure 7*D*). Thus, as observed in vitro, ZO-1 deletion leads to defective orientation of the mitotic spindle in vivo. Taken as a whole, these data show a critical contribution of ZO-1 to mitotic spindle orientation in vivo and explain the means by which ZO-1 loss results in abortive proliferation and ineffective mucosal repair.

Discussion

ZO-1 was the first epithelial tight junction protein identified,[24] but it is also expressed in cells that do not form tight junctions, including blastomeres at the 8-cell stage of mammalian development.[25] This contrasts with some other tight junction proteins whose expression is limited to epithelial and endothelial cells and whose knockout induces only subtle abnormalities.[26–28] In contrast, knockout of *Tjp1*, which encodes ZO-1, leads to the developmental defects as early as embryonic day 8.5, extensive apoptosis of neuroectodermal tissues, failure of vascular development, and embryonic death.[10] ZO-1 must, therefore, have critical functions separate from tight junctions. Consistent with this, ZO-1 knockdown or knockout in cell lines did not prevent tight junction assembly or development of barrier function.[15,29,30]

ZO-1$^{KO.IEC}$ mice were born, grew, and gained weight normally; did not develop spontaneous disease; and displayed only a mild increase in leak pathway permeability. This suggests that mice are able to compensate for ZO-1 loss via mechanisms that do not depend on altered steady-state expression of other tight junction proteins. To unmask potentially critical ZO-1 functions in intestinal epithelia, ZO-1$^{KO.IEC}$ mice were challenged using 3 distinct approaches. The results, which were consistent across all 3 models, showed enhanced mucosal damage, defective repair, and sustained inflammatory responses in ZO-1$^{KO.IEC}$ mice relative to WT littermates.

Our studies identified 2 separate, but synergistic, effects of ZO-1 loss. First, ZO-1–deficient epithelial cells were deficient in activation of proliferative, such as Wnt–β-catenin, and repair pathways after injury. This correlates with in vivo and in vitro proliferative defects in intestinal epithelial stem cells but contrasts sharply with previous in vitro studies showing accelerated growth of Madin-Darby canine kidney (MDCK) and embryonic stem cells after ZO-1 knockdown or knockout, respectively.[29–31] Our studies suggest that these divergent results are not merely due to differences between in vivo and in vitro

Figure 7. ZO-1 associates with spindle poles in vitro and is required for effective mitosis in vivo. (*A*) Colonoids from vil-mRFP1-ZO-1^{Tg} mice were labeled with NucSpot (*red*). ZO-1 (*green*) surface contours were generated from 3-dimensional stacks. A representative mitotic event with ZO-1 localization at the spindle poles (*arrows*) is shown. The lower row of drawings is presented to assist with interpretation of the 3-dimensional image projections. (*B*) Immunostains of small intestinal epithelia show ZO-1 (*green*) foci within the subapical cytoplasm. These overlap with pericentrin (*red; sites of overlap are highlighted by blue circles*), demonstrating that ZO-1 localizes to the centriole and pericentriolar apparatus in interphase intestinal epithelia. (*C*) After 6 days of treatment with 2% DSS, mice were returned to water; injected with EdU (*green*); and sacrificed 4, 24, and 48 hours later. Increases in labeled cell numbers between 4 and 24 hours were far greater in WT, relative to ZO-1$^{KO.IEC}$, colonic epithelium. Consistent with abortive proliferation, the number of apoptotic colonocytes with fragmented EdU staining increased markedly in ZO-1$^{KO.IEC}$, but not WT, mice. n = 4 per group. (*D*) Tissue sections from WT and ZO-1$^{KO.IEC}$ mice receiving water or 2% DSS were labeled for NuMA (*green*), E-cadherin (*red*), ZO-1 (*yellow*), and nuclei (*blue*). Mitotic events with 2 distinct NuMA foci showed spindle misorientation in ZO-1$^{KO.IEC}$ (*red*) relative to WT (*blue*) mice. n = 4–8 per group. Scale bars: (*A*) 5 μm; (*B*) 5 μm; (*C*) 40 μm; (*D*) 20 μm or 10 μm (high magnification). Analysis of variance with Bonferroni correction. *P < .05; ***P < .001.

growth conditions. Moreover, we confirmed that the phenotypes observed are the result of ZO-1 loss because transgenic mRFP1-ZO-1 expression rescued proliferation in ZO-1–knockout intestinal stem cells. ZO-1 loss therefore creates an epithelial-intrinsic proliferative deficit that is, at least in part, due to defective Wnt pathway activation. Although the molecular events responsible for this abnormality remain to be defined, the observations that ZO-1 can bind directly to α-catenin[32] and that expression of a truncated ZO-1 protein lacking the α-catenin-binding GuK domain in MDCK cells, which causes epithelial-mesenchymal transition, activates β-catenin signaling[33] provide some potential clues as to the underlying mechanism. In contrast, the in vivo defects observed here are distinct from the reported association of ZO-1 with MRCKβ at the leading edge of migrating nonpolarized cells.[34]

At baseline, neither EdU incorporation nor MKI67 expression, both markers of dividing cells, were altered in ZO-1$^{KO.IEC}$ mice. This suggests that, in the absence of stress, intestinal epithelia lacking ZO-1 are able to proliferate at a level sufficient to maintain homeostasis despite reduced expression of Wnt pathway genes. However, ZO-1$^{KO.IEC}$ mice were unable to up-regulate growth factor-induced proliferation after injury. This observation also explains the in vitro growth defect observed in colonoids because these cells are grown with media that contains growth factors including Wnt, R-spondin, epidermal growth factor, and noggin.

Although profound, the proliferative failure could not explain the increased apoptotic rates of ZO-1–deficient intestinal epithelia. Live imaging of colonoids showed that ZO-1 deletion resulted in mitotic spindle misorientation. This caused 1 daughter cell to lose contact with the basement membrane and undergo anoikis or mitotic catastrophe–associated apoptosis. This resulted in an abortive proliferative process that failed to produce additional viable cells but did generate an excess of cleaved caspase-3–positive apoptotic cells.

Although the mechanisms by which DSS and TNBS induce colitis are incompletely defined, the protection afforded by reduced epithelial caspase-3 expression (in occludin-knockout mice)[4] indicates that caspase-3–dependent apoptosis is central to both. Moreover, the apoptosis of ZO-1–deficient intestinal epithelia induced by growth-promoting stimuli, both in vivo and in vitro, correlates with the massive apoptosis that occurs within rapidly dividing neuroectodermal tissues of ZO-1–knockout embryos.[10] Thus, although speculative, the data could support the idea that ZO-1 is primarily required under conditions where cell division must be accelerated. Delayed mitotic spindle orientation in ZO-1–deficient epithelia could therefore explain the consequences of ZO-1 loss in both unstressed and stressed mice.

The observed spindle misorientation is similar to our previous in vitro report of multilumen formation in ZO-1–knockdown MDCK cells grown in 3-dimensional culture.[30] We did not, however, detect multilumen enteroids or colonoids (not shown). One possible explanation could be that this reflects the difference between nonimmortalized epithelial cells, such as those within colonoids, that undergo anoikis upon detachment from the basement membrane and immortalized cell lines are capable of anchorage-independent growth. In the latter, anchorage-independent outgrowths resulting from misoriented mitosis could be the origin of the septae that divide cysts into multiple lumens.

Our previous in vitro studies did not provide insight into the means by which ZO-1 directs mitotic spindle orientation. Here, we used live imaging to demonstrate a transient association between ZO-1 and spindle poles and immunostains to document the presence of ZO-1 within interphase centrioles. This was unexpected, because ZO-1 has not been previously reported to associate with the centrosome or bind directly to microtubules. Nevertheless, together with reports linking centrioles and primary cilia to Wnt, Hedgehog, and Notch signaling as well as microfilament organization (including microvilli),[35–37] a potential regulatory function of ZO-1 at centrosomes could integrate the seemingly disparate phenotypes observed in ZO-1–deficient epithelia.

As a whole, these data should prompt the reevaluation of studies in which a correlation between ZO-1 down-regulation and increased intestinal permeability has led to the conclusion that there is a causal relationship. Our studies definitively demonstrate that ZO-1 is not required for barrier function and that, in the absence of stress, intestinal epithelia can compensate for ZO-1 loss. Nevertheless, ZO-1 is critical to epithelial repair and contributes to both Wnt–β-catenin signaling and mitotic spindle orientation. It is, therefore, likely that the ZO-1 down-regulation in human and experimental inflammatory bowel disease compromises mucosal repair and, in doing so, promotes disease progression. Interventions that overcome these consequences of ZO-1 loss may, therefore, provide new means of enhancing mucosal healing and promoting the resolution of active disease.

Supplementary Material

Note: To access the supplementary material accompanying this article, visit the online version of *Gastroenterology* at www.gastrojournal.org, and at https://doi.org/10.1053/j.gastro.2021.08.047.

References

1. Wyatt J, Vogelsang H, Hubl W, et al. Intestinal permeability and the prediction of relapse in Crohn's disease. Lancet 1993;341:1437–1439.
2. Hollander D, Vadheim CM, Brettholz E, et al. Increased intestinal permeability in patients with Crohn's disease and their relatives. A possible etiologic factor. Ann Intern Med 1986;105:883–885.
3. **Turpin W, Lee SH**, Raygoza Garay JA, et al. Increased intestinal permeability is associated with later development of Crohn's disease. Gastroenterology 2020;159:2092–2100.

4. **Kuo WT, Shen L**, Zuo L, et al. Inflammation-induced occludin downregulation limits epithelial apoptosis by suppressing caspase-3 expression. Gastroenterology 2019;157:1323–1337.
5. Kucharzik T, Walsh SV, Chen J, et al. Neutrophil transmigration in inflammatory bowel disease is associated with differential expression of epithelial intercellular junction proteins. Am J Pathol 2001;159:2001–2009.
6. Heller F, Florian P, Bojarski C, et al. Interleukin-13 is the key effector Th2 cytokine in ulcerative colitis that affects epithelial tight junctions, apoptosis, and cell restitution. Gastroenterology 2005;129:550–564.
7. Zeissig S, Burgel N, Gunzel D, et al. Changes in expression and distribution of claudin 2, 5 and 8 lead to discontinuous tight junctions and barrier dysfunction in active Crohn's disease. Gut 2007;56:61–72.
8. Noble CL, Abbas AR, Cornelius J, et al. Regional variation in gene expression in the healthy colon is dysregulated in ulcerative colitis. Gut 2008;57:1398–1405.
9. Nalle SC, Zuo L, Ong M, et al. Graft-versus-host disease propagation depends on increased intestinal epithelial tight junction permeability. J Clin Invest 2019;129:902–914.
10. Katsuno T, Umeda K, Matsui T, et al. Deficiency of zonula occludens-1 causes embryonic lethal phenotype associated with defected yolk sac angiogenesis and apoptosis of embryonic cells. Mol Biol Cell 2008;19:2465–2475.
11. Odenwald MA, Choi W, Kuo WT, et al. The scaffolding protein ZO-1 coordinates actomyosin and epithelial apical specializations in vitro and in vivo. J Biol Chem 2018;293:17317–17335.
12. **Kieckhaefer J, Lukovac S**, Ye DZ, et al. The RNA polymerase III subunit Polr3b is required for the maintenance of small intestinal crypts in mice. Cell Mol Gastroenterol Hepatol 2016;2:783–795.
13. Tsai PY, Zhang B, He WQ, et al. IL-22 upregulates epithelial claudin-2 to drive diarrhea and enteric pathogen clearance. Cell Host Microbe 2017;21:671–681.
14. Chanez-Paredes SD, Abtahi S, Kuo W-T, et al. Differentiating between tight junction-dependent and tight junction-independent intestinal barrier loss in vivo. Methods Mol Biol 2021;2367:249–271.
15. **Van Itallie CM, Fanning AS**, Bridges A, et al. ZO-1 stabilizes the tight junction solute barrier through coupling to the perijunctional cytoskeleton. Mol Biol Cell 2009;20:3930–3940.
16. **Raju P, Shashikanth N**, Tsai PY, et al. Inactivation of paracellular cation-selective claudin-2 channels attenuates immune-mediated experimental colitis in mice. J Clin Invest 2020;130:5197–5208.
17. Clayburgh DR, Barrett TA, Tang Y, et al. Epithelial myosin light chain kinase-dependent barrier dysfunction mediates T cell activation-induced diarrhea in vivo. J Clin Invest 2005;115:2702–2715.
18. Mansilla S, Priebe W, Portugal J. Mitotic catastrophe results in cell death by caspase-dependent and caspase-independent mechanisms. Cell Cycle 2006;5:53–60.
19. Gottardi CJ, Arpin M, Fanning AS, et al. The junction-associated protein, zonula occludens-1, localizes to the nucleus before the maturation and during the remodeling of cell-cell contacts. Proc Natl Acad Sci U S A 1996;93:10779–10784.
20. Van Itallie CM, Aponte A, Tietgens AJ, et al. The N and C termini of ZO-1 are surrounded by distinct proteins and functional protein networks. J Biol Chem 2013;288:13775–13788.
21. Marchiando AM, Shen L, Graham WV, et al. Caveolin-1-dependent occludin endocytosis is required for TNF-induced tight junction regulation in vivo. J Cell Biol 2010;189:111–126.
22. Bacallao R, Antony C, Dotti C, et al. The subcellular organization of Madin-Darby canine kidney cells during the formation of a polarized epithelium. J Cell Biol 1989;109:2817–2832.
23. Merdes A, Heald R, Samejima K, et al. Formation of spindle poles by dynein/dynactin-dependent transport of NuMA. J Cell Biol 2000;149:851–862.
24. Stevenson BR, Siliciano JD, Mooseker MS, et al. Identification of ZO-1: a high molecular weight polypeptide associated with the tight junction (zonula occludens) in a variety of epithelia. J Cell Biol 1986;103:755–766.
25. Fleming TP, McConnell J, Johnson MH, et al. Development of tight junctions de novo in the mouse early embryo: control of assembly of the tight junction-specific protein, ZO-1. J Cell Biol 1989;108:1407–1418.
26. **Paschoud S, Bongiovanni M**, Pache JC, et al. Claudin-1 and claudin-5 expression patterns differentiate lung squamous cell carcinomas from adenocarcinomas. Mod Pathol 2007;20:947–954.
27. Matsumoto K, Imasato M, Yamazaki Y, et al. Claudin 2 deficiency reduces bile flow and increases susceptibility to cholesterol gallstone disease in mice. Gastroenterology 2014;147:1134–1145.
28. Guillemot L, Schneider Y, Brun P, et al. Cingulin is dispensable for epithelial barrier function and tight junction structure, and plays a role in the control of claudin-2 expression and response to duodenal mucosa injury. J Cell Sci 2012;125:5005–5014.
29. Xu J, Lim SB, Ng MY, et al. ZO-1 regulates Erk, Smad1/5/8, Smad2, and RhoA activities to modulate self-renewal and differentiation of mouse embryonic stem cells. Stem Cells 2012;30:1885–1900.
30. Odenwald MA, Choi W, Buckley A, et al. ZO-1 interactions with F-actin and occludin direct epithelial polarization and single lumen specification in 3D culture. J Cell Sci 2017;130:243–259.
31. Balda MS, Garrett MD, Matter K. The ZO-1–associated Y-box factor ZONAB regulates epithelial cell proliferation and cell density. J Cell Biol 2003;160:423–432.
32. Itoh M, Nagafuchi A, Moroi S, et al. Involvement of ZO-1 in cadherin-based cell adhesion through its direct binding to α catenin and actin filaments. J Cell Biol 1997;138:181–192.
33. **Reichert M, Muller T**, Hunziker W. The PDZ domains of zonula occludens-1 induce an epithelial to mesenchymal transition of Madin-Darby canine kidney I cells. Evidence

for a role of β-catenin/Tcf/Lef signaling. J Biol Chem 2000;275:9492–9500.
34. Huo L, Wen W, Wang R, et al. Cdc42-dependent formation of the ZO-1/MRCKβ complex at the leading edge controls cell migration. EMBO J 2011;30:665–678.
35. Campos Y, Qiu X, Gomero E, et al. Alix-mediated assembly of the actomyosin–tight junction polarity complex preserves epithelial polarity and epithelial barrier. Nat Commun 2016;7:11876.
36. Kyun M-L, Kim S-O, Lee HG, et al. Wnt3a stimulation promotes primary ciliogenesis through β-catenin phosphorylation-induced reorganization of centriolar satellites. Cell Rep 2020;30:1447–1462.
37. Akhshi T, Trimble WS. A non-canonical Hedgehog pathway initiates ciliogenesis and autophagy. J Cell Biol 2021;220(1):e202004179.

Author names in bold designate shared co-first authorship.

Received July 22, 2021. Accepted August 26, 2021.

Correspondence
Address correspondence to: Jerrold R. Turner, MD, PhD, Brigham and Women's Hospital, 77 Avenue Louis Pasteur, HNRB 752L, Boston, Massachusetts 02115. e-mail: jrturner@bwh.harvard.edu.

CRediT Authorship Contributions
Wei-Ting Kuo, PhD (Conceptualization: Lead; Investigation: Lead; Writing – original draft: Lead; Writing – review & editing: Lead); Li Zuo, PhD (Investigation: Equal; Writing – original draft: Equal; Writing – review & editing: Equal); Matthew A. Odenwald, MD, PhD (Investigation: Supporting; Writing – review & editing: Supporting); Shariq Madha, PhD (Formal analysis: Supporting); Gurminder Singh, MA (Investigation: Supporting; Writing – review & editing: Supporting); Christine B. Gurniak, PhD (Resources: Supporting); Clara Abraham, MD (Formal analysis: Supporting; Writing – review & editing: Supporting); Jerrold R. Turner, MD, PhD (Conceptualization: Lead; Formal analysis: Lead; Funding acquisition: Lead; Investigation: Supporting; Writing – original draft: Lead; Writing – review & editing: Lead).

Acknowledgments
The authors thank Tiffany S. Davanzo (Slaybaugh Studios) for her beautiful illustrations and Heather Marlatt (Nationwide Histology) for her outstanding assistance with histologic staining and tissue microarray development.

Wei Ting Kuo's current affiliation is the Graduate Institute of Oral Biology, National Taiwan University, Taipei, Taiwan. Gurminder Singh's current affiliation is AbbVie Inc, Cambridge, Massachusetts.

Conflicts of interest
Guminder Singh is an employee of AbbVie, Inc. Jerrold R. Turner is a founder and shareholder of Thelium Therapeutics and has served as a consultant for Entrinsic, Immunic, and Kallyope. The remaining authors disclose no conflicts.

Funding
This work was supported by National Institutes of Health grants R01DK61931 (to Jerrold R. Turner), R01DK68271 (to Jerrold R. Turner), R01DK099097 (to Clara Abraham), and P30DK034854 (to the Harvard Digestive Disease Center) and by the National Natural Science Foundation of China grants 81800464 (to Li Zuo) and 82070548 (to Li Zuo).